Nonlinear generation of hollow beams in tunable plasmonic nanosuspensions

Cite as: APL Photon. 8, 076102 (2023); doi: 10.1063/5.0153856
Submitted: 12 April 2023 • Accepted: 8 June 2023 •
Published Online: 5 July 2023

Jingyan Zhan,[1] Denghui Li,[2] Domenico Bongiovanni,[1,3] Yinxiao Xiang,[4] Shengyao Chen,[1] Yujie Zhang,[1] Liqin Tang,[1] Daohong Song,[1] Jianke Yang,[5] Roberto Morandotti,[3] and Zhigang Chen[1,a)]

AFFILIATIONS

[1] The MOE Key Laboratory of Weak-Light Nonlinear Photonics, TEDA Applied Physics Institute, and School of Physics, Nankai University, Tianjin 300457, China
[2] State Key Laboratory of NBC Protection for Civilian, Research Institute of Chemical Defense, Beijing 102205, China
[3] INRS-EMT, 1650 Blvd. Lionel-Boulet, Varennes, Quebec J3X 1S2, Canada
[4] Department of Physics and Astronomy, West Virginia University, Morgantown, West Virginia 26506, USA
[5] Department of Mathematics and Statistics, University of Vermont, Burlington, Vermont 05405, USA

[a)] **Author to whom correspondence should be addressed:** zgchen@nankai.edu.cn

ABSTRACT

We experimentally demonstrate that a probe beam at one wavelength, although exhibiting a weak nonlinear response on its own, can be modulated and controlled by a pump beam at another wavelength in plasmonic nanosuspensions, leading to ring-shaped pattern generation. In particular, we show that the probe and pump wavelengths can be interchanged, but the hollow beam patterns appear only in the probe beam, thanks to the gold nanosuspensions that exhibit a strong nonlinear response to pump beam illumination at the plasmonic resonant frequencies. Colloidal suspensions consisting of either gold nanospheres or gold nanorods are employed as nonlinear media, which give rise to refractive index changes and cross-phase modulation between the two beams. We perform a series of experiments to examine the dynamics of hollow beam generation at a fixed probe power as the pump power is varied and find that nonlinear beam shaping has a different power threshold in different nanosuspensions. Our results will enhance the understanding of nonlinear light–matter interactions in plasmonic nanosuspensions, which may be useful for applications in controlling light by light and in optical limiting.

I. INTRODUCTION

Over the past few decades, colloidal suspensions and soft matter in general have attracted a great deal of interest due to their potential applications in a variety of fields ranging from life sciences to chemistry, physics, as well as photonics.[1–9] Of particular interest are synthetic and artificial materials that exhibit novel nonlinear optical properties such as dielectric nanoparticle suspensions.[10–15] Various synthetic materials with extraordinary nonlinear properties have been demonstrated for applications in photonic devices including optical modulators and optical switches.[16–21] Plasmonic nanosuspensions, for instance, have been proposed and tested as an ideal material candidate for applications in nonlinear optics.[22–30] Such colloidal systems are particularly interesting due to the fact that the optical response of suspended metallic nanoparticles is mediated by a localized surface plasmon resonance (SPR) and can be readily tuned through composition, size, and shape.[22,31–33] The tunable optical nonlinearity in plasmonic nanosuspensions exhibits superior performance, as compared to their dielectric counterparts, in supporting beam guidance and self-trapping.[22,23,28,29,34]

In colloidal suspensions of metallic nanoparticles, robust soliton-like propagation has been observed due to an effective cubic–quintic-like plasmonic resonant nonlinearity.[26,34–37] The wavelength-dependent nonlinear response can be used to explore promising photonic applications based on controlling light by light. Interestingly, a plasmonic nanosuspension can be used as a tunable nonlinear medium in which the refractive index changes along the beam path, for instance, when a Gaussian-like beam of a particular wavelength is launched through it. As a result, a nonlinear phase shift occurs on another beam that is collinearly propagating.

The process of phase shift in one beam modulated by intensity-dependent index changes in another beam is the well-known cross-phase modulation (XPM), which has been intensively investigated for controlling light-by-light technologies.[38–41] Yet, most of the previous endeavors have been focused mainly on the context of nonlinear optical fibers, liquid crystals, or conventional nonlinear materials.[42–47] One may wonder what advantages and new features could emerge when a plasmonic resonant nonlinearity comes to play a role.

On the other hand, "hollow" Gaussian beams have been extensively investigated due to their special intensity distribution and propagation characteristics[48,49] and have attracted much attention in the research fields of atom manipulation,[50–52] optical trapping,[53–55] and plasma physics.[56–59] The propagation and transformation dynamics of a hollow beam in nonlinear media have also been explored for potential applications in optical limiting[60] and high-energy laser propagation.[61] Various methods for generating hollow beams have been proposed and demonstrated, such as employing spatial filtering, beam shaping, optical fibers, and the nonlinear interaction of photons with orbital angular momentum.[62–65] A natural question is if the nonlinear response of plasmonic suspensions to light excitations can bring about a new possibility for the generation of hollow beams. Specifically, can the XPM mentioned earlier be used to induce hollow beam formation in metallic nanosuspensions, taking advantage of their plasmonic resonant nonlinearity?

In this work, we propose and demonstrate nonlinear hollow beam generation in plasmonic nanosuspensions. We analyze and discuss wavelength-dependent nonlinear optical responses in two typical gold nanoparticle (nanosphere and nanorod) suspensions. Experimentally, we observe that a low-power probe beam propagating in colloidal gold nanosuspensions can be modulated and controlled by a pump beam at a different wavelength, resulting in an unexpected nonlinear reshaping of its initial intensity profile into a doughnut-like pattern. We find that the probe and pump wavelengths can be interchanged by using different gold nanosuspensions (for instance, we can have a green beam for the pump and an infrared beam for the probe for nanosphere suspension, but the same infrared beam for the pump and the green beam for the probe for nanorod suspension), yet the hollow pattern only appears in the probe beam , which does not exhibit a strong nonlinear response on its own. Furthermore, our experimental results are also corroborated by numerical simulations using coupled nonlinear Schrödinger equations (NLSEs) involving the XPM effect from the two copropagating optical beams.

II. MATERIALS AND METHODS

A. Wavelength-dependent nonlinear response

To explore the optical properties of plasmonic nanosuspensions, it is crucial to have a good understanding of the response of individual nanoparticles to an optical field. SPR dominates the optical response of metallic nanoparticles and depends critically on their size, shape, and composition, as well as the optical properties of the irradiating beam laser, including the wavelength, polarization, and intensity.[22,31,66] In previous studies, the SPR of independent metal nanoparticles induced by an external electromagnetic field has been characterized by polarization, absorption, and scattering cross sections, whose spectral evolutions associated with these physical parameters reach their maximum value when the field wavelength approaches the SPR frequency. In addition, it is possible to achieve polarization contrast in specified spectral regions by selecting the proper polarization-dependent composite film comprised of metal nanoparticles.[67–69] Furthermore, plasmonic nanosuspensions illuminated by a light with a frequency near the SPR give rise to changes in the refractive index occurring in the proximity of the beam path. By appropriately engineering the main components of plasmonic colloids, we can straightforwardly tune the associated wavelength-dependent nonlinear optical responses, thus controlling the flow of light in soft-matter systems. In what follows, we shall investigate the nonlinear response in colloidal suspensions of two exemplary plasmonic gold nanoparticles (see Fig. 1) and demonstrate experimentally their suitability as a nonlinear medium to control light by light.

Two transmission electron microscopy (TEM) images in Figs. 1(a1) and 1(b1) illustrate the geometrical properties of plasmonic nanoparticles used in our experimental characterization, consisting of gold nanospheres (with an average diameter of 40 nm) and gold nanorods (with an average diameter and length of 12 and 78 nm, respectively). From the TEM images, it is also evident that the two different types of gold nanoparticles are not aggregated in water, but they exhibit a high degree of dispersion. First, the main components in the colloidal suspensions of gold nanospheres are analyzed. As seen in Figs. 1(a2) and 1(a3), a gold nanosphere particle with such a small diameter exhibits the maximum peak of the plasmon resonance response near a wavelength of 532 nm. In this case, the real part of the polarizability α_R and the light absorption cross section acquire large values when gold nanospheres in suspension are illuminated by a pump beam operating at 532 nm. Furthermore, the curve of polarization plotting the imaginary part α_{IM} also takes relatively large values at the same wavelength, thus unveiling high absorption loss. As a result, the interplay between optical gradient forces $\vec{F}_{\mathrm{grad}} = (1/4)\alpha_R \nabla \left|\vec{E}\right|^2$ (which are dependent on α_{R}) and nonlocal nonlinear defocusing (which is related to light absorption), along with the low scattering forces, causes a significant variation of refractive index along the beam path, which happens in two different ways according to the sign of the particle polarizability at the pump wavelength.[26,70–72] On the other hand, compared with their isotropic counterparts like gold nanoshells and nanospheres, gold nanorods feature two main axes: transverse (along the short axis **b**) and longitudinal (along the long axis **a**), as shown in the inset in Fig. 1(b2). Their anisotropic shape induces a splitting of the SPR into transverse and longitudinal SPR modes,[25,27,73,74] corresponding to perpendicular and parallel polarizations of the external electromagnetic field, respectively. The related perpendicular polarizability $\alpha_\perp$ and parallel polarizability $\alpha_\parallel$ are described by the following expression:[25,75]

$$\alpha_{\parallel,\perp} = 4\pi ab^2 \varepsilon_m \frac{\varepsilon_1 - \varepsilon_m}{3\varepsilon_m + 3L_{\parallel,\perp}(\varepsilon_1 - \varepsilon_m)}, \tag{1}$$

where ε_1 and ε_{m} are, respectively, the frequency-dependent complex dielectric constants of the gold nanosphere and the surrounding medium, and they can be described by the Drude-Lorentz

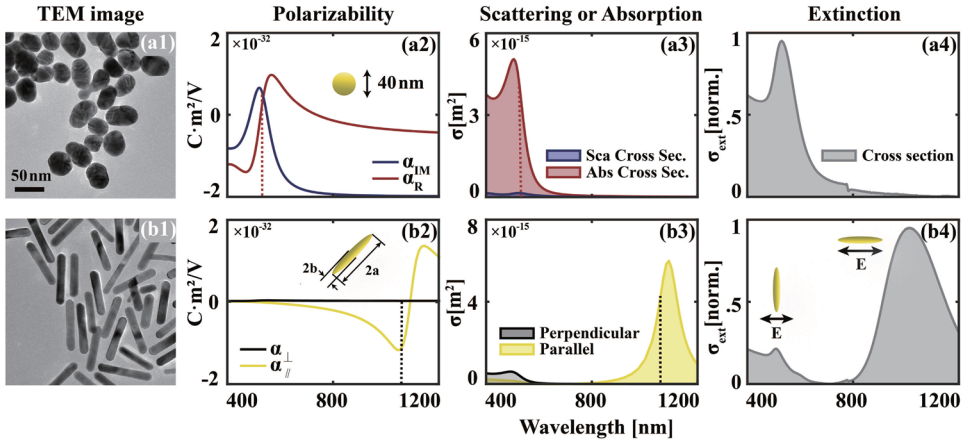

FIG. 1. (a1) and (b1) TEM images for (a1) gold nanospheres (sample 1) and (b1) gold nanorods (sample 2). (a2) and (b2) Polarizability spectra of gold nanosuspensions in aqueous solution. The red and blue curves in (a2) plot the calculated real (α_R) and imaginary (α_{IM}) parts of polarizability for gold nanospheres, while the yellow and black curves in (b2) indicate the parallel ($\alpha_\parallel$) and perpendicular ($\alpha_\perp$) real parts of anisotropic polarizability for gold nanorods, respectively. (a3) Calculated absorption (solid red line) and scattering (solid blue line) cross sections of a single gold nanosphere. (b3) Calculated parallel (solid yellow line) and perpendicular (solid black line) absorption cross sections of a single gold nanorod. The red dotted lines in (a2) and (a3) and the black dotted lines in (b2) and (b3) mark the wavelengths at 532 and 1064 nm, respectively. (a4) and (b4) Measured normalized extinction cross-sections for samples in (a1) and (b1), respectively.

model. The geometrical structure factor along the longitudinal mode direction is given by

$$L_\parallel = \frac{1-e^2}{e^2}\left(\frac{1}{2e}\ln\frac{1+e}{1-e}-1\right), \tag{2}$$

where the eccentricity e is defined as $e^2 = 1 - b^2/a^2$. Instead, the geometric factor along the short axis is $L_\perp = \left(1 - L_\parallel\right)/2$. Applying the above-mentioned equations, the calculated values of the polarizabilities as a function of wavelength are shown in Fig. 1(b2). Whereas the the component in the perpendicular direction (black line) of polarizability generally maintains a positive value over a broad range of wavelengths, the component in the parallel direction (yellow line) varies considerably in both sign and amplitude around the characteristic plasmon resonance frequency (approximately located at 1064 nm). It is noteworthy that, when the wavelength shifts to the near-infrared (NIR), the parallel components of both polarizability and absorption cross sections are much larger than the perpendicular ones [see Figs. 1(b2) and 1(b3)], indicating that the longitudinal SPR mode is dominant at that time. In addition, this behavior is also consistent with our experimental observations, as discussed in Sec. III. Remarkably, it is also noticed that the polarizability in suspensions of gold nanospheres at 532 nm and gold nanorods at 1064 nm feature opposite signs, and there are two different nonlinear mechanisms responsible for changing the refractive index at low pump power. In both cases, the refractive index along the pump path increases, and therefore the light-particle interaction leads to a nonlinear optical response for these two wavelengths. However, at very high pump power, thermal effects will dominate the nonlinear response phenomenon.

Besides, we also obtained experimentally the extinction spectra of two nanosuspension samples under examination. The combined absorption-extinction measurements are often used to characterize the optical properties of plasmonic nanosuspensions, where the extinction spectrum is the sum of the absorption and scattering of light by the metal nanoparticles.[22,76] The instrument used for measurement is a broad-spectrum spectrophotometer (Hitachi U-4100), and the characterization is performed by illuminating the two samples with incoherent white light. Measurements are presented in Figs. 1(a4) and 1(b4), and they refer to normalized results for the case of a colloidal suspension of nanospheres and nanorods, respectively. According to these measurements, we found that the gold nanosphere in suspension manifests an intense extinction effect near the wavelength of 532 nm. This result is consistent with the value previously obtained in simulations, and it is also indicative of the fact that a 532 nm pump leads to a significant nonlinear response for this soft matter. Meanwhile, the pairs of peaks appearing in the extinction spectrum of the gold nanorod suspension can be attributed to the transverse and longitudinal SPR modes, highlighting that the overall wavelength-dependent extinction effect of the plasmonic nanosuspension is the collective manifestation of an individual nanorod. One can see clearly that the peak value of the extinction cross section related to the longitudinal mode is much larger than that of the transverse mode, and as a consequence, the gold nanorod exhibits a strong nonlinear response near the wavelength of 1064 nm. Therefore, for the sample filled with gold nanorods, we use the laser wavelength of 1064 nm as the pump beam for our experimental characterization.

B. Experimental setup

A schematic representation of the experimental setup used for observing the hollow-beam formation due to nonlinear beam coupling in plasmonic suspensions is shown in Fig. 2. A 30 mm-long quartz cuvette filled with a 5 ml mixture of the aqueous gold nanosuspensions (XFNANO Producer: No. XFJ6 7440-57-5 for the nanosphere suspension and No. XFJ61 7440-57-5 for the nanorod suspension; whose uniform concentration of these samples is about

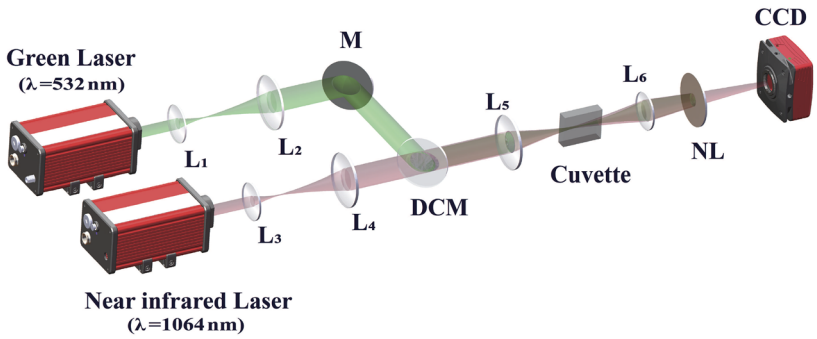

FIG. 2. Schematic illustration of the experimental setup. A linearly polarized NIR beam at 1064 nm and a green beam at 532 nm propagate collinearly through a sample (a 30 mm-long cuvette; particle concentration: 0.05 mg/ml) containing a gold nanosuspension. The roles of "pump" and "probe" for these two beams can be interchanged, as discussed in the text. The lenses (L1, L2) and (L3, L4) before the dichroic mirrors are responsible for linearly expanding the two beams. L5, focusing lenses (f = 120 mm); L6, imaging lens; DCM, dichroic mirror; M, mirror; NF, notch filter. The images of input/output intensity patterns are taken by the CCD camera.

0.05 mg/ml) is inserted in the optical path. When the sample containing gold nanosphere suspensions is examined, the continuous-wave (CW) laser operating at λ = 532 nm (green) acts as the pump beam, while the other CW laser source at the NIR wavelength (λ = 1064 nm) serves as the probe. On the contrary, the pump and probe beams are switched when the sample with gold nanorod suspensions is tested. In order to induce a plasmonic resonant optical nonlinearity, the pump beam is focused inside the cuvette directly in the plasmonic solution, and its focal point position is about 10 mm from the front surface of the cuvette. The pump power can be varied from 0 to 300 mW. Meanwhile, the probe beam is injected collinearly with the pump, and its input power is fixed at 5 mW for all sets of measurements. Before being focused on the sample, the collinear pump and probe beams are combined by a dichroic mirror. Due to the very low power, the probe beam does not experience nonlinear self-action itself in the plasmonic suspension. The probe intensity pattern at the output face of the sample is then measured by means of a notch filter in order to remove the high-intensity pump light. A CCD camera is employed to record the output intensity profiles of the probe beam for various input pump powers. In addition, as the notch filter obstructing the pump beam is replaced, the output intensity pattern of the pump beam when the hollow beam is generated can also be measured. Both nonlinearly-induced hollow beams and probe-beam guidance are verified by simply recording their corresponding output pattern images.

III. EXPERIMENTAL RESULTS OF NONLINEAR HOLLOW BEAM GENERATION

From the direct examination of the output intensity profiles of the probe beam for every experimental setting, the formation of hollow patterns in gold nanosuspension is observed to take place over a wide range of pump powers, from 30 to 250 mW. As seen in Figs. 3 and 4, our experimental results conducted in an aqueous suspension containing either gold nanospheres with a 40 nm average diameter or gold nanorods with a 6.5 aspect ratio demonstrate the generation of hollow beams under different wavelengths and power conditions.

A. Experimental results in nanosphere suspension

In gold nanosphere suspensions, the pump beam is focused on the plasmonic sample at different input powers and experiences plasmonic resonant optical nonlinearity, while the collinear NIR probe beam is fixed at a low power of 5 mW to prevent nonlinear self-action. Experimental results in Figs. 3(b1)–3(b6) show clearly that the initial Gaussian-like intensity pattern of the NIR probe beam converts into a hollow-shaped beam after passing through the gold nanosphere suspension, especially under intense pump irradiations. In the linear regime of the pump beam, the low-power probe undergoes normal diffraction and does not exhibit an hollow pattern, as shown in Fig. 3(b1). However, as the pump power increases above a certain threshold value, nonlinear coupling takes place in the suspensions, and the probe beam propagating collinearly with the pump is guided and starts to deform and differ from the fundamental Gaussian pattern at the output, as shown in Fig. 3(b2). For higher pump powers, the probe-beam intensity progressively evolves into a hollow pattern. In particular, the hollow pattern appears for values higher than 30 mW, with both the ring radius and the hollow size varying with the pump power. Meanwhile, the output intensity patterns of the pump beam are also recorded by means of a notch filter [see Figs. 3(a1) and 3(a2)]. Only two output intensity patterns measured at two specific powers are presented for convenience in the illustration. For a relatively high power, one can see that the increasing tendency of the output pump size indicates a negative or self-defocusing response, although no hollow pattern is observed for the pump itself; this is a nonlinear effect that is mainly caused by a plasmon resonance. The self-defocusing nonlinearity of nanoparticle suspension under continuous light illumination has been verified by Z-scan experiments.[70–72]

B. Experimental results in nanorod suspension

Subsequently, the formation of nonlinearly-induced hollow beams is also observed in nanorod suspensions (see Fig. 4). In this case, the power threshold at which the hollow shaped pattern appears increases with respect to that in the nanospheres suspension. Comparing Figs. 3(b2) and 4(b3), the necessary pump power

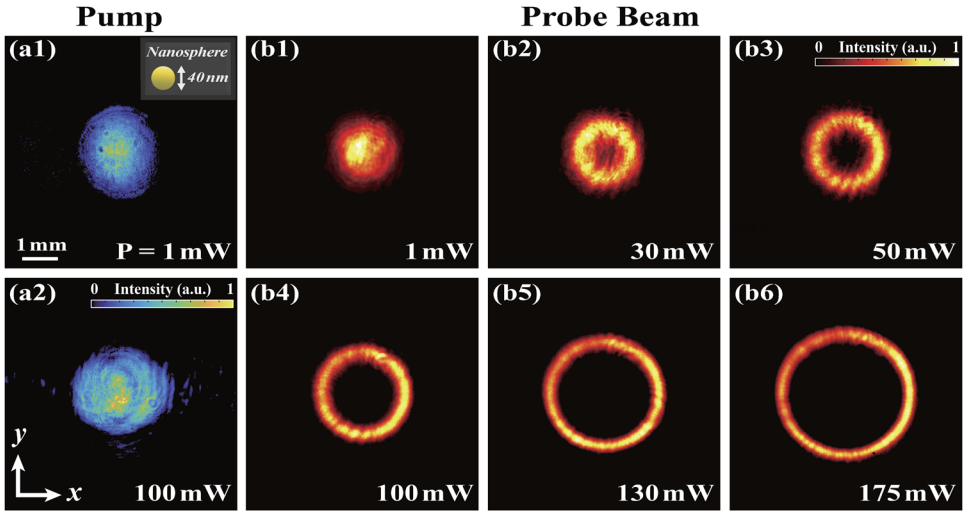

FIG. 3. Experimental observations showing hollow beam generation in a nonlinear gold-nanosphere suspension. (a1) and (a2) Output intensity patterns of the green pump beam at 532 nm after 30 mm-long propagation in the sample for low and high input power: (a1) 1 mW and (a2) 100 mW. (b1)–(b6) Output intensity patterns recorded for the NIR probe beam (whose power is fixed at $P_{probe1064}$ = 5 mW) at different pump powers.

to create an evident hollow-beam pattern is significantly different for nanosphere and nanorod suspensions. This difference is mainly attributed to the nonlinear optical properties of the samples as well as a slight difference in the waist sizes of the two probe beams. However, when only the NIR pump beam is present, the output intensity patterns are consistent with previously obtained experimental results for gold nanosphere suspension. The dark-region size of the induced hollow beam is power dependent in the plasmon nanosuspension. In addition, we have also carried out additional experiments by using a gold nanorod suspension with a plasmon resonance at 810 nm (off from both pump and probe wavelengths) for a direct comparison, as shown in Fig. S3 in the supplementary material, thus highlighting the need for a plasmonic enhancement to initiate the nonlinear effect. At increasing pump powers, the dark region of the hollow beam becomes larger, indicating that gold nanosuspensions have a tunable nonlinear response within a certain range. We note that tunable hollow beams have demonstrated superior stability and efficiency in particle trapping and

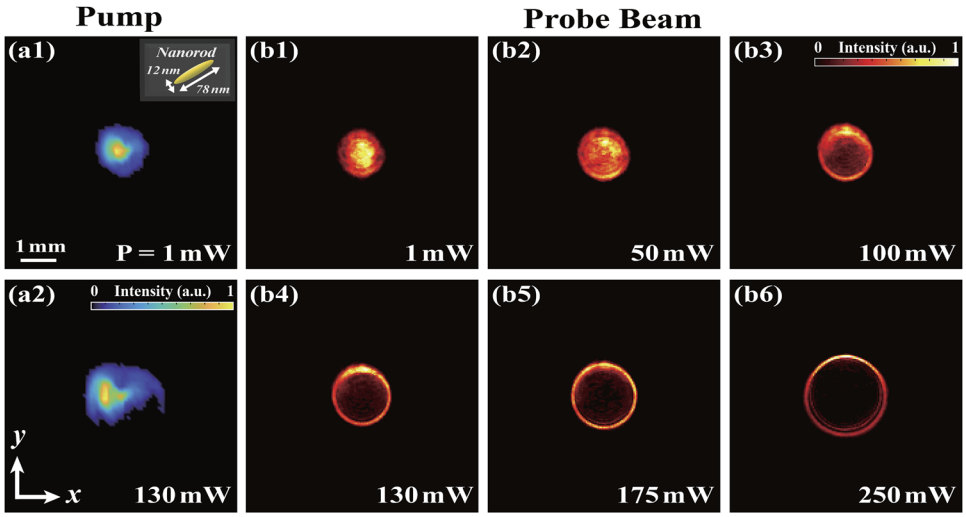

FIG. 4. Experimental results showing hollow beam generation in a nonlinear gold nanorod suspension. (a1) and (a2) Output intensity patterns of the NIR pump beam at 1064 nm after 30 mm-long propagation in the sample at input powers of (a1) 1 mW and (a2) 130 mW. (b1)–(b6) Output intensity patterns of the green probe beam at 532 nm (whose power is now fixed at 5 mW) for various pump powers of the NIR beam.

manipulation applications.[55,77] Here, the dimensions of the hollow beam can be modulated according to the pump power as well as the size of the particle, thus offering great potential for particle manipulation and non-invasive diagnosis.[53,78]

IV. DISCUSSION

To confirm that the observed nonlinear response is the result of a surface plasmon resonance, we did a series of comparison experiments. First, the same experiment is carried out in a pure aqueous solution without immersing any gold nanoparticles, and in this case, no appreciable nonlinear action on either the probe or the pump beam is observed, thus excluding the influence of the solution itself. Second, we carried out the same experiment by using a gold nanorod suspension with a plasmon resonance off both the pump and the probe wavelengths. In this latter case, the output intensities of the probe beam (again with fixed low power at 5 mW) do not exhibit a pronounced hollow pattern generation as the NIR pump power increases, indicating that the nonlinear response is mediated by the plasmonic resonant absorption.

The observed phenomenon can be better explained by beam interaction through cross-phase modulation (XPM). XPM is an important nonlinear optical process that occurs when the nonlinear response induced by the presence of one optical beam affects the dynamic of the other. If two light beams with the same or different wavelengths pass through a nonlinear medium, one beam intensity influences the refractive index of the medium, which in turn modulates the other beam phase. XPM generally occurs in nonlinear media, especially in materials with third-order nonlinearity, which acts as a mechanism of beam phase modulation in a suitable nonlinear medium.[38,39,41] In optical pulse transmission, for example, ultrafast optical switches can be studied by employing a phase shift induced by XPM; ultrafast pulses can be re-timed through XPM; and the time and space characteristics of ultrafast pulses can also be controlled via XPM. This nonlinear effect has been widely applied to soliton formation, pulse compression, and spectrum broadening in recent years.[39,79,80] In this section, the nonlinear phenomena in our experimental observations are numerically simulated with physical parameters from the experiment, attaining a good degree of consistency between them. The correlated propagation dynamics can be described under the paraxial approximation condition by the following coupled NLSEs:

$$\begin{aligned} i\frac{\partial}{\partial z}\psi_1 + \frac{1}{2k_1 n_0}\nabla_\perp^2\psi_1 &= -k_1 n_2\left(|\psi_1|^2 + 2|\psi_2|^2\right)\psi_1, \\ i\frac{\partial}{\partial z}\psi_2 + \frac{1}{2k_2 n_0}\nabla_\perp^2\psi_2 &= -k_2 n_2\left(|\psi_2|^2 + 2|\psi_1|^2\right)\psi_2, \end{aligned} \tag{3}$$

where $\psi_j(\mathrm{r})$ (j = 1 and 2) are the electric field envelopes of two co-propagating optical waves, denoted as pump and probe beam, respectively, while k_j represents their wavenumber, and n_0 is the background refractive index of the medium. As two beams interact with a nonlinear medium, the changes in the refractive index due to the third-order nonlinear refractive coefficient n_2 corresponding to a wavelength λ_j can be written in a more compact

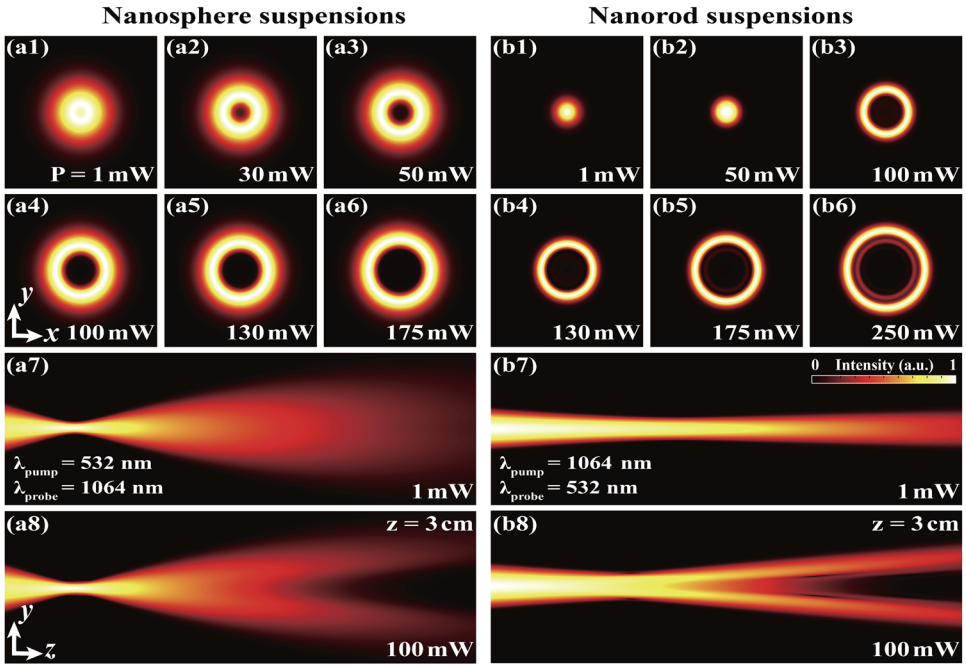

FIG. 5. Numerical results showing hollow beam generation in a nonlinear gold nanosuspensions induced by cross-phase modulation (XPM). (a1)–(a6) Output intensity patterns of a NIR probe beam (power fixed at $P_{probe1064}$ = 5 mW) for various pump powers of the green beam in gold nanosphere suspensions. (a7) and (a8) Side-view propagation of the probe beam at pump powers of (a7) 1 mW and (a8) 100 mW. (b1)–(b6) Corresponding output intensity patterns for gold nanorod suspensions obtained by switching the wavelengths of the probe to 532 nm (while fixing its power at $P_{probe532}$ = 5 mW) and the pump beam to 1064 nm. (b7) and (b8) Same as (a7) and (a8) except for the nanorod suspensions.

form as $\Delta n_j = n_2\left(|\psi_j|^2 + 2|\psi_{3-j}|^2\right)$. We assume in Eq. (3) that the two Gaussian beam profiles are initially described as $\psi_j(r) = \sqrt{2P_j/\pi\omega_{0j}^2}\exp\left(-r^2/\omega_{0j}^2\right)$, where P_j is the input power and ω_{0j} is the beam waist. Numerical simulations are performed by using Eq. (3) with parameters chosen according to the experimental conditions: $\omega_{01} = \omega_{02} = 0.06$ mm for nanorods (0.075 mm for nanospheres) $\lambda_1 = 1064$ nm, $\lambda_2 = 532$ nm, $n_2 = -1 \times 10^{-13}$. From a physical viewpoint, local refractive index changes take place as the gold nanosuspensions are irradiated by intense pumping light, and the weak collinearly propagating probe beam experiences an additional phase modulation, which impresses the hollow beam pattern. As shown in Fig. 5, numerical results are in qualitatively good agreement with the experimental observations in Figs. 3 and 4. Furthermore, the propagation dynamics of the probe beam under different pump excitations [see Figs. 5(a7), (a8), (b7), and (b8)] highlight the influence of a high pump power, which significantly affects the probe beam propagation as compared to the low power regime where diffraction is predominant. While the mechanisms for nonlinear self-guiding in nanoparticle suspensions merit further and deeper investigation, our numerical results confirm the expectation that hollow beams are engendered by the action of nonlinear XPM.

V. CONCLUSIONS

In summary, we have demonstrated tunable hollow beam generation in nonlinear plasmonic nanosuspensions, illustrating an example that plasmonic gold nanosuspensions represent a versatile platform for controlling the flow of light in soft-matter systems. We have shown the wavelength-dependent nonlinear optical response of gold nanosphere and nanorod suspensions, and then we observed that a low-power probe beam can be reshaped and controlled by a high-power pump beam over 30 mm-long propagation through the plasmonic nanosuspensions. Furthermore, we have illustrated the cross-phase modulation effect of two beams in the nonlinear medium, which indicates that plasmonic nanosuspensions have great potential for all-optical limiting and switching. We envision that more exotic structured beams can also be designed and created in a variety of optical systems with plasmonic resonant interactions. These results will not only add insight into nonlinear optics with plasmonic nanosuspensions but may also offer an effective plasmonic platform for all-optical signal-processing technologies and devices.

SUPPLEMENTARY MATERIAL

The supplementary material includes additional experimental results in pure aqueous solution without immersing any Au nanoparticle, other conditions for nonlinear beam propagation in different plasmonic nanosuspensions for direct comparisons, as well as data from calculations for a single gold nanorod particle.

ACKNOWLEDGMENTS

We acknowledge Trevor Kelly and Huizhong Xu for insightful discussion.

This research was funded by the National Key R&D Program of China (Grant No. 2022YFA1404800), the National Natural Science Foundation of China (Grant Nos. 12134006 and 11922408), and the Natural Science Foundation of Tianjin (Grant No. 21JCJQJC00050). D.B. acknowledges support from the 66 Postdoctoral Science Grant of China and the National Natural Science Foundation (Grant No. 12250410236). R.M. acknowledges support from NSERC and the CRC research program. J.Y. acknowledges support from NSF grant (DMS-1910282).

AUTHOR DECLARATIONS

Conflict of Interest

The authors have no conflicts to disclose.

Author Contributions

J.Z., D.L., and D.B. contributed equally to this work.

Jingyan Zhan: Conceptualization (equal); Data curation (equal); Methodology (equal); Software (equal); Validation (equal); Visualization (equal); Writing – original draft (equal). **Denghui Li**: Conceptualization (equal); Investigation (lead); Software (equal); Supervision (lead); Validation (equal). **Domenico Bongiovanni**: Formal analysis (equal); Writing – original draft (equal). **Yinxiao Xiang**: Validation (equal). **Shengyao Chen**: Formal analysis (equal). **Yujie Zhang**: Formal analysis (equal). **Liqin Tang**: Writing – review & editing (equal). **Daohong Song**: Writing – review & editing (equal). **Jianke Yang**: Writing – review & editing (equal). **Roberto Morandotti**: Supervision (supporting); Writing – review & editing (supporting). **Zhigang Chen**: Funding acquisition (equal); Project administration (equal); Resources (equal); Supervision (equal); Writing – review & editing (equal). All authors contributed to the editing of the manuscript.

DATA AVAILABILITY

All source data that support the plots within this paper and other findings of this study are available from the corresponding authors upon reasonable request.

REFERENCES

[1] H. Löwen, "Colloidal soft matter under external control," J. Phys.: Condens. Matter **13**, R415 (2001).
[2] L. De Sio *et al.*, "Universal soft matter template for photonic applications," Soft Matter **7**, 3739–3743 (2011).
[3] A. Bezryadina *et al.*, "Nonlinear self-action of light through biological suspensions," Phys. Rev. Lett. **119**, 058101 (2017).
[4] S. Loescher *et al.*, "3D DNA origami nanoparticles: From basic design principles to emerging applications in soft matter and (bio-)nanosciences," Angew. Chem., Int. Ed. **57**, 10436–10448 (2018).
[5] R. Gautam *et al.*, "Nonlinear optical response and self-trapping of light in biological suspensions," ADV PHYS-X **5**, 1778526 (2020).
[6] P. Christopher *et al.*, "Visible-light-enhanced catalytic oxidation reactions on plasmonic silver nanostructures," Nat. Chem. **3**, 467–472 (2011).
[7] C. Majidi, "Soft-matter engineering for soft robotics," Adv. Mater. Technol. **4**, 1800477 (2019).

[8]U. R. Gabinet and C. O. Osuji, "Optical materials and metamaterials from nanostructured soft matter," Nano Res. **12**, 2172–2183 (2019).
[9]Y. Chen *et al.*, "Soft optical metamaterials," Nano Converg. **7**, 18 (2020).
[10]C. Conti *et al.*, "Optical spatial solitons in soft matter," Phys. Rev. Lett. **95**, 183902 (2005).
[11]R. El-Ganainy *et al.*, "Soliton dynamics and self-induced transparency in nonlinear nanosuspensions," Opt. Express **15**, 10207–10218 (2007).
[12]M. Matuszewski *et al.*, "Spatial solitons and light-induced instabilities in colloidal media," Opt. Express **16**, 1371–1376 (2008).
[13]E. Greenfield *et al.*, "Shockwave based nonlinear optical manipulation in densely scattering opaque suspensions," Opt. Express **21**, 23785–23802 (2013).
[14]W. Man *et al.*, "Optical nonlinearities and enhanced light transmission in soft-matter systems with tunable polarizabilities," Phys. Rev. Lett. **111**, 218302 (2013).
[15]S. Fardad *et al.*, "Interactions between self-channeled optical beams in soft-matter systems with artificial nonlinearities," Opt. Lett. **38**, 3585–3587 (2013).
[16]Y. Dong *et al.*, "Saturable absorption in 2D Ti_3C_2 mxene thin films for passive photonic diodes," Adv. Mater. **30**, 1705714 (2018).
[17]L. Wu *et al.*, "Few-layer tin sulfide: A promising black-phosphorus-analogue 2D material with exceptionally large nonlinear optical response, high stability, and applications in all-optical switching and wavelength conversion," Adv. Opt. Mater. **6**, 1700985 (2018).
[18]L. Wu *et al.*, "2D tellurium based high-performance all-optical nonlinear photonic devices," Adv. Funct. Mater. **29**, 1806346 (2019).
[19]L. Wu *et al.*, "Kerr nonlinearity in 2D graphdiyne for passive photonic diodes," Adv. Mater. **31**, 1807981 (2019).
[20]C. Zhang *et al.*, "Anisotropic nonlinear optical properties of a snse flake and a novel perspective for the application of all-optical switching," Adv. Opt. Mater. **7**, 1900631 (2019).
[21]L. Wu *et al.*, "1D@0D hybrid dimensional heterojunction-based photonics logical gate and isolator," Appl. Mater. Today **19**, 100589 (2020).
[22]S. Fardad *et al.*, "Plasmonic resonant solitons in metallic nanosuspensions," Nano Lett. **14**, 2498–2504 (2014).
[23]T. S. Kelly *et al.*, "Guiding and nonlinear coupling of light in plasmonic nanosuspensions," Opt. Lett. **41**, 3817–3820 (2016).
[24]A. S. Reyna and C. B. de Araújo, "High-order optical nonlinearities in plasmonic nanocomposites-a review," Adv. Opt. Photonics **9**, 720–774 (2017).
[25]Y.-X. Ren *et al.*, "Soliton-mediated orientational ordering of gold nanorods and birefringence in plasmonic suspensions," Opt. Lett. **42**, 627–630 (2017).
[26]V. Shvedov *et al.*, "Nonlinear propagation and quasi self-confinement of light in plasmonic resonant media," Opt. Express **26**, 23196–23206 (2018).
[27]H. Xu *et al.*, "Plasmonic resonant nonlinearity and synthetic optical properties in gold nanorod suspensions," Photonics Res. **7**, 28–35 (2019).
[28]Y. Xiang *et al.*, "Resonant optical nonlinearity and fluorescence enhancement in electrically tuned plasmonic nanosuspensions," Adv. Photonics Res. **2**, 2000060 (2021).
[29]A. Balbuena Ortega *et al.*, "Guiding light with singular beams in nanoplasmonic colloids," Appl. Phys. Lett. **118**, 061102 (2021).
[30]K. Sivashanmugan *et al.*, "Biological photonic crystal-enhanced plasmonic mesocapsules: Approaching single-molecule optofluidic-sers sensing," Adv. Opt. Mater. **7**, 1900415 (2019).
[31]S. A. Kalele *et al.*, "Plasmon-assisted photonics at the nanoscale," J. Nanophotonics **1**, 012501 (2007).
[32]Y. Xia *et al.*, "Shape-controlled synthesis of metal nanocrystals: Simple chemistry meets complex physics?," Angew. Chem., Int. Ed. **48**, 60–103 (2009).
[33]M. R. Gonçalves, "Plasmonic nanoparticles: Fabrication, simulation and experiments," J. Phys. D: Appl. Phys. **47**, 213001 (2014).
[34]A. S. Reyna and C. B. de Araújo, "Guiding and confinement of light induced by optical vortex solitons in a cubic-quintic medium," Opt. Lett. **41**, 191–194 (2016).
[35]E. L. Falcão-Filho *et al.*, "High-order nonlinearities of aqueous colloids containing silver nanoparticles," J. Opt. Soc. Am. B **24**, 2948–2956 (2007).
[36]E. L. Falcão-Filho *et al.*, "High-order nonlinearity of silica-gold nanoshells in chloroform at 1560 nm," Opt. Express **18**, 21636–21644 (2010).
[37]A. S. Reyna and C. B. de Araújo, "Nonlinearity management of photonic composites and observation of spatial-modulation instability due to quintic nonlinearity," Phys. Rev. A **89**, 063803 (2014).
[38]Z.-B. Wang *et al.*, "Large cross-phase modulation between slow copropagating weak pulses in ^{87}Rb," Phys. Rev. Lett. **97**, 063901 (2006).
[39]Y. Shen *et al.*, "Nonlinear cross-phase modulation with intense single-cycle terahertz pulses," Phys. Rev. Lett. **99**, 043901 (2007).
[40]B.-W. Shiau *et al.*, "Low-light-level cross-phase modulation with double slow light pulses," Phys. Rev. Lett. **106**, 193006 (2011).
[41]L. Cheng *et al.*, "Manipulation of a ring-shaped beam via spatial self- and cross-phase modulation at lower intensity," Phys. Chem. Chem. Phys. **21**, 7618–7622 (2019).
[42]M. N. Islam *et al.*, "Cross-phase modulation in optical fibers," Opt. Lett. **12**, 625–627 (1987).
[43]J. Cho *et al.*, "Shaping lightwaves in time and frequency for optical fiber communication," Nat. Commun. **13**, 785 (2022).
[44]A. S. Ostrovsky *et al.*, "Generation of the 'perfect' optical vortex using a liquid-crystal spatial light modulator," Opt. Lett. **38**, 534–536 (2013).
[45]Y. Shen *et al.*, "Field alignment of bent-core smectic liquid crystals for analog optical phase modulation," Appl. Phys. Lett. **106**, 191101 (2015).
[46]J. U. Kang *et al.*, "Observation of manakov spatial solitons in algaas planar waveguides," Phys. Rev. Lett. **76**, 3699–3702 (1996).
[47]Z. Chen *et al.*, "Coupled photorefractive spatial-soliton pairs," J. Opt. Soc. Am. B **14**, 3066–3077 (1997).
[48]Y. Cai *et al.*, "Hollow Gaussian beams and their propagation properties," Opt. Lett. **28**, 1084–1086 (2003).
[49]Y. Zhou *et al.*, "Propagation of hollow vortex Gaussian beams in a strongly nonlocal nonlinear media," Laser Phys. **28**, 105003 (2018).
[50]T. Kuga *et al.*, "Novel optical trap of atoms with a doughnut beam," Phys. Rev. Lett. **78**, 4713–4716 (1997).
[51]Y. B. Ovchinnikov *et al.*, "Surface trap for Cs atoms based on evanescent-wave cooling," Phys. Rev. Lett. **79**, 2225–2228 (1997).
[52]J. Yin *et al.*, "Atom guiding and cooling in a dark hollow laser beam," Phys. Rev. A **58**, 509–513 (1998).
[53]A. P. Porfirev and R. V. Skidanov, "Dark-hollow optical beams with a controllable shape for optical trapping in air," Opt. Express **23**, 8373–8382 (2015).
[54]B. Tang *et al.*, "Radiation force of highly focused modified hollow Gaussian beams on a Rayleigh particle," Optik **127**, 6446–6451 (2016).
[55]Z. Liu *et al.*, "Enhancement of trapping efficiency by utilizing a hollow sinh-Gaussian beam," Sci. Rep. **9**, 10187 (2019).
[56]A. Sharma *et al.*, "Dynamics of dark hollow Gaussian laser pulses in relativistic plasma," Phys. Rev. E **87**, 063111 (2013).
[57]G. Purohit *et al.*, "Second harmonic generation by self-focusing of intense hollow Gaussian laser beam in collisionless plasma," Phys. Plasmas **23**, 013103 (2016).
[58]P. Rawat *et al.*, "Generation of terahertz radiation by intense hollow Gaussian laser beam in magnetised plasma under relativistic-ponderomotive regime," Phys. Plasmas **24**, 073113 (2017).
[59]X.-R. Hong *et al.*, "Propagation characteristics of a hollow Gaussian laser beam in a tapered plasma channel," Phys. Plasmas **27**, 043109 (2020).
[60]L. Lu and Z. Wang, "Hollow Gaussian beam: Generation, transformation and application in optical limiting," Opt. Commun. **471**, 125809 (2020).
[61]L. Lu *et al.*, "Thermal blooming induced phase change and its compensation of a Gaussian beam propagation in an absorbing medium," Opt. Lett. **46**, 4304–4307 (2021).
[62]Z. Liu *et al.*, "Generation of hollow Gaussian beams by spatial filtering," Opt. Lett. **32**, 2076–2078 (2007).
[63]Y. Nie *et al.*, "Generation of dark hollow femtosecond pulsed beam by phase-only liquid crystal spatial light modulator," Appl. Opt. **50**, 4174–4179 (2011).
[64]C. Zhao *et al.*, "Generation of a high-quality partially coherent dark hollow beam with a multimode fiber," Opt. Lett. **33**, 1389–1391 (2008).
[65]N. A. Chaitanya *et al.*, "Hollow Gaussian beam generation through nonlinear interaction of photons with orbital angular momentum," Sci. Rep. **6**, 32464 (2016).
[66]H. Chen *et al.*, "Shape- and size-dependent refractive index sensitivity of gold nanoparticles," Langmuir **24**, 5233–5237 (2008).

[67]S. G. Moiseev, "Thin-film polarizer made of heterogeneous medium with uniformly oriented silver nanoparticles," Appl. Phys. A **103**, 775–777 (2011).
[68]S. G. Moiseev, "Nanocomposite-based ultrathin polarization beamsplitter," Opt. Spectrosc. **111**, 233–240 (2011).
[69]V. G. Bordo, "Theory of light reflection and transmission by a plasmonic nanocomposite slab: Emergence of broadband perfect absorption," J. Opt. Soc. Am. B **38**, 1442–1451 (2021).
[70]A. Balbuena Ortega *et al.*, "Light control through a nonlinear lensing effect in a colloid of biosynthesized gold nanoparticles," J. Mod. Opt. **66**, 502–511 (2019).
[71]L. Sarkhosh *et al.*, "Large thermally induced nonlinear refraction of gold nanoparticles stabilized by cyclohexanone," Phys. Status Solidi A **207**, 2303–2310 (2010).
[72]A. Balbuena Ortega *et al.*, "Nonlocal nonlinear refractive index of gold nanoparticles synthesized by ascorbic acid reduction: Comparison of fitting models," J. Mod. Opt. **61**, S68–S73 (2014).
[73]J. Li *et al.*, "Microscopic and macroscopic manipulation of gold nanorod and its hybrid nanostructures [invited]," Photonics Res. **1**, 28–41 (2013).
[74]J.-W. Liaw *et al.*, "Wavelength-dependent longitudinal polarizability of gold nanorod on optical torques," Opt. Express **22**, 10858–10867 (2014).
[75]P. V. Ruijgrok *et al.*, "Brownian fluctuations and heating of an optically aligned gold nanorod," Phys. Rev. Lett. **107**, 037401 (2011).
[76]J. Grand *et al.*, "Combined extinction and absorption uv–visible spectroscopy as a method for revealing shape imperfections of metallic nanoparticles," Anal. Chem. **91**, 14639–14648 (2019).
[77]Z. Gong *et al.*, "Characterization of single airborne particle extinction using the tunable optical trap-cavity ringdown spectroscopy (OT-CRDS) in the uv," Opt. Express **25**, 6732–6745 (2017).
[78]B. He *et al.*, "Particle trapping and manipulation using hollow beam with tunable size generated by thermal nonlinear optical effect," Appl. Phys. Express **11**, 052501 (2018).
[79]O. Cohen *et al.*, "Cross-phase-modulation nonlinearities and holographic solitons in periodically poled photovoltaic photorefractives," Opt. Lett. **31**, 954–956 (2006).
[80]M. Spanner *et al.*, "Tunable optimal compression of ultrabroadband pulses by cross-phase modulation," Opt. Lett. **28**, 749–751 (2003).